

# Permian–Triassic magmatism in response to Palaeotethys subduction and pre-Late Triassic arrival of northeast Gondwana-derived continental fragments at the southern Eurasian margin: detrital zircon evidence from Triassic sandstones of Central Iran

Guido Meinhold <sup>a,b\*</sup>, Seyyedeh Halimeh Hashemi Azizi <sup>c</sup>, Jasper Berndt <sup>d</sup>

<sup>a</sup> *School of Geography, Geology and the Environment, Keele University, Keele, Staffordshire, ST5 5BG, United Kingdom*

<sup>b</sup> *Geowissenschaftliches Zentrum der Universität Göttingen, Abteilung Sedimentologie und Umweltgeologie, Goldschmidtstraße 3, D-37077 Göttingen, Germany*

<sup>c</sup> *Department of Geology, Faculty of Sciences, 3995 University of Hormozgan, Bandar Abbas, Iran*

<sup>d</sup> *Institut für Mineralogie, Westfälische Wilhelms-Universität Münster, Corrensstraße 24, D-48149 Münster, Germany*

\* Corresponding author at: School of Geography, Geology and the Environment, Keele University, Keele, Staffordshire, ST5 5BG, United Kingdom.

E-mail address: [g.meinhold@keele.ac.uk](mailto:g.meinhold@keele.ac.uk) (G. Meinhold).

## Abstract

The closure of Palaeotethys that led to the collision of the Cimmerian blocks with the southern Eurasian margin causing the Eo-Cimmerian orogeny during the Early Mesozoic is still controversially discussed. The Triassic Nakhlak Group in Central Iran is a key sedimentary succession for better understanding the closure of Palaeotethys and the Eo-Cimmerian orogeny in the Middle East. The Nakhlak Group is composed of the Alam (Olenekian to Middle Anisian), Baqoroq (?Upper Anisian to Middle Ladinian) and Ashin (Upper Ladinian to ?Carnian) formations, which consist mainly of volcanoclastic sandstones, mixed siliciclastic conglomerates, and marine carbonates. Here we present for the first time detrital zircon U–Pb ages from the Nakhlak Group to unravel its provenance and constrain its palaeotectonic position within the Palaeotethyan realm. Most detrital zircons from the Nakhlak Group are euhedral and subhedral with Permian–Triassic ages (ca. 280–240 Ma) suggesting sediment supply from Permian–Triassic magmatic rocks of the Silk Road Arc. Minor zircon populations show pre-Permian Palaeozoic ages, with age peaks at ca. 320 Ma and 480 Ma, which are probably derived from the basement on which the magmatic arc developed. Neoproterozoic–latest Mesoproterozoic (ca. 550–1100 Ma) and Palaeoproterozoic (ca. 1800–2200 Ma) zircon grains are anhedral (rounded). The latter are prominent in the upper Baqoroq Formation (Middle Ladinian) suggesting recycling of older sedimentary rocks. Sandstone petrography points toward an additional metamorphic provenance for this formation. This short-lived provenance change can be explained by tectonic uplift in the source area that led to erosion of metamorphosed rocks

with a northeast Gondwanan affinity. It clearly indicates that northeast Gondwana-derived continental fragments likely belonging to the Cimmerian blocks already arrived at the southern Eurasian margin in pre-Late Triassic time. Current palaeotectonic models of the closure of Palaeotethys and the Eo-Cimmerian orogeny in the Middle East during the Triassic may need to be revised.

*Keywords:* zircon U–Pb ages; Triassic; Central Iran; Eo-Cimmerian orogeny; Palaeotethys

## 1. Introduction

The region stretching from the Eastern Mediterranean to central and southeast Asia experienced severe tectonic reorganization during the Palaeozoic and Mesozoic eras due to the opening and closure of the Palaeo- and Neotethys oceans (Stöcklin, 1968; Şengör, 1979, 1984; Şengör et al., 1988; Stampfli, 2000; Stampfli and Borel, 2002; Stampfli and Kozur, 2006; Muttoni et al., 2009a,b; Natal'in et al., 2016) (Fig. 1a). Subduction of Palaeotethys beneath the southern Eurasian margin in Late Palaeozoic and Early Mesozoic times led to the formation of magmatic arc systems, the most prominent being the long-lived Silk Road Arc defined by Natal'in and Şengör (2005) (Fig. 1b). The arc system was built mostly on subduction–accretion complexes of Middle to Late Palaeozoic age (Natal'in and Şengör, 2005). Related magmatic rocks stretch from the southwestern Black Sea region (e.g., Strandja Massif in NW Turkey; Natal'in et al., 2016) through the Greater Caucasus and northern Iran and continue through North Pamir and Kuen–Lun, to the Qilian Shan and beyond (Şengör, 1984; Şengör and Natal'in, 1996; Natal'in and Şengör, 2005). Magmatic activity of the Silk Road Arc in the Scythian and Turan domains vanished when Palaeotethys closed and the Cimmerian blocks, also known as the Cimmerian continent (Şengör, 1979), collided with Eurasia in the Late Triassic (Şengör, 1979, 1984; Şengör et al., 1988; Stampfli, 2000; Garzanti and Gaetani, 2002; Stampfli and Kozur, 2006; Wilmsen et al., 2009; Zanchi et al., 2009a).

The Silk Road Arc was accompanied by trench-slope, fore-arc, intra-arc and back-arc basins. In Iran, remnants of these basins and thus of the Palaeotethys can be traced through the northeast, around Mashhad and eastward to Aghdarband, and in the Anarak–Nakhlak region located in the northwest part of the Central-East Iranian Microcontinent (CEIM), consisting largely of the Yazd, Tabas and Lut continental blocks and the Anarak–Jandaq terrane, south of the Great Kavir–Doruneh Fault (Baud et al., 1991; Bagheri and Stampfli, 2008; Zanchi et al., 2009a,b, 2015; Buchs et al., 2013; Zanchetta et al., 2013) (Fig. 2). The CEIM is part of Central Iran, also named Central Iranian Plateau, according to Beberian and King (1981). The palaeogeographic location of the Anarak–Nakhlak region in Mesozoic time is still being debated. Davoudzadeh et al. (1981) suggested that the Palaeotethys-related units of the CEIM were displaced from the present-day Afghan–Iranian border region after the Triassic, reaching their position after a 135° anticlockwise rotation of the CEIM (Soffel et al., 1996). However, the reliability of their palaeomagnetic data has been questioned by Muttoni et al. (2009b).

In this study, we focus on the Triassic Nakhlak Group in the Nakhlak region of Central Iran (Figs. 2–4) as it can be regarded as a key area for understanding the diminish of Palaeotethys and the arrival of the Cimmerian blocks and their collision with the southern Eurasian margin. The dominantly siliciclastic sedimentary succession of the Nakhlak Group

differs from coeval strata in the surrounding regions which mainly comprise carbonate platform facies (Alavi et al., 1997; Seyed-Emami, 2003). It shows resemblances with the Triassic Aghdarband Group in northeastern Iran, east of Kopeh-Dagh (Fig. 2), with Eurasian affinity (Davoudzadeh et al., 1981; Baud and Stampfli, 1989; Baud et al., 1991; Ruttner, 1984, 1991, 1993; Alavi et al., 1997), although both groups were not deposited close to each other (Balini et al., 2009, 2019). The Naxhlak Group was deposited in a fore-arc basin (e.g., Alavi et al., 1997) whereas the Triassic Aghdarband Group was deposited in a back-arc basin (e.g., Baud et al., 1991; Balini et al., 2019). The Naxhlak Group is nowadays located in the NW part of the CEIM which has a Cimmerian affinity (Stöcklin, 1968; Şengör, 1979, 1990).

For many years, uncertainty concerning the palaeotectonic evolution of Central Iran including the Naxhlak Group has mainly because of lack of hard data (e.g., provenance data) for testing the various palaeotectonic models. Balini et al. (2009) and Zanchi et al. (2009b) presented sandstone petrographic data to discuss the provenance of the clastic sediments. Recently, Hashemi Azizi et al. (2018a,b) presented new petrographic data together with whole-rock geochemical and mineral chemical data. All of these studies suggest a magmatic arc provenance; however, the middle part of the Naxhlak Group received prominent sediment supply from upper crustal metamorphic source rocks. Zircon U–Pb geochronology has been widely used as a tool in sedimentary provenance analysis to unravel source areas, sediment transport pathways, and the maximum age of deposition of siliciclastic sedimentary successions (e.g., Horton et al., 2008; Meinhold et al., 2011; Moghadam et al., 2017). Such data are unavailable for the Triassic Naxhlak Group.

This study provides the first detrital zircon U–Pb ages for a provenance study of the Triassic Naxhlak Group sandstones to constrain the origin and the palaeoposition of the Naxhlak Group within the Palaeotethyan realm. The new provenance data allow to better constrain the closure of the Palaeotethys and the arrival of the Cimmerian blocks at the southern Eurasian margin during the Early Mesozoic.

## **2. Geological setting**

The Naxhlak Group is exposed in a NW–SE trending mountain ridge to the west of the village and mine of Naxhlak (Fig. 3). The ~2700-m-thick sedimentary succession of the Naxhlak Group (Fig. 4) is unconformably overlain by an up to ~260-m-thick Upper Cretaceous succession (Vaziri et al., 2005, 2012). In the studied section, the contact between the Triassic and Cretaceous is of tectonic nature.

The Naxhlak Group is composed of volcanoclastic sandstones, mixed siliciclastic conglomerates, and marine carbonates (Fig. 4). It has been subdivided from the base to top into three formations (Davoudzadeh and Seyed-Emami, 1972): the Alam Formation (Olenekian to Middle Anisian), the Baqoroq Formation (?Upper Anisian to Middle Ladinian), and the Ashin Formation (Upper Ladinian to ?Carnian) (see also Vaziri and Fürsich, 2007). The Naxhlak Group lies with a tectonic contact above pre-Triassic metamorphic mafic and ultramafic rocks. They are not well exposed and only small outcrops can be identified in the southernmost part of the area. The mafic rocks comprise amphibole-metagabbros whereas the ultramafic rocks are represented by serpentinites (Zanchi et al., 2009b). The rock assemblage is commonly interpreted as a dismembered ophiolitic complex of Middle–Late Palaeozoic age, i.e. Naxhlak-

type ophiolite of Bagheri and Stampfli (2008). According to Bagheri and Stampfli (2008), the mafic–ultramafic rock assemblage is the basement of the Triassic Palaeotethyan fore-arc basin. Zanchi et al. (2009b) emphasize that no clear evidence for an oceanic lithosphere within the Nakhlak-type ophiolite has been given yet.

The sedimentary rocks of the Triassic Nakhlak Group have been described in detail by Davoudzadeh and Seyed-Emami (1972), Alavi et al. (1997), Seyed-Emami (2003), Vaziri and Fürsich (2007), Balini et al. (2009), Zanchi et al. (2009b) and Hashemi Azizi et al. (2018a,b). Below we provide a brief summary and refer to the cited literature for details.

The Alam Formation is a 1060-m-thick mixed clastic and calcareous succession (Fig. 4) comprising volcanoclastic sandstone beds, minor conglomerates, calcareous massive layers and fossiliferous limestones including mud mounds (Berra et al., 2012), deposited in an agitated shallow marine environment. Petrographic analysis of thin sections (i.e. modal analysis via point counting) revealed that most of the sandstone samples from the Alam Formation include dominantly volcanic detritus mainly represented by lithic fragments and single phenocrysts such as volcanic quartz grains and feldspars (Hashemi Azizi et al., 2018a). The average total quartz–feldspar–lithic fragment ratio is Qt21.6:F38.7:L39.7 (Hashemi Azizi et al., 2018a).

The Baqoroq Formation lies with an erosive contact above the Alam Formation (Fig. 4). Although it is barren from any types of fossils, a ?Late Anisian–Middle Ladinian age has been assigned to this formation considering its stratigraphic position between the Alam and Ashin formations (Davoudzadeh and Seyed-Emami, 1972; Vaziri and Fürsich, 2007; Balini et al., 2009). The 1294-m-thick Baqoroq formation starts with a conglomerate bed consisting of ooid grainstone pebbles (Fig. 4), probably originated from the Alam Formation, and continues into a succession of red, massive, clast-supported conglomerates and coarse-grained sandstones (Fig. 4). Fining-upward sequences composed of conglomerates, sandstones and shale beds are well-developed in the middle part toward the top of the formation. The coarse lithologies and sedimentary structures (e.g., imbrication and trough cross-beds) demonstrate a gravel-bed fluvial depositional environment. Generally, the Baqoroq Formation can be subdivided into a lower and an upper part (Fig. 4). Such subdivision has already been recognized by Alavi et al. (1997). The lower part comprises first-cycle sedimentary and volcanic material as well as some recycled metamorphic basement (Hashemi Azizi et al., 2018a). The upper part comprises less sedimentary and volcanic material and is chiefly composed of low-grade metamorphic detritus (Zanchi et al., 2009b; Hashemi Azizi et al., 2018a). Baqoroq Formation sandstones have an average total quartz–feldspar–lithic fragment ratio of Qt45:F19.7:L35.3 (Hashemi Azizi et al., 2018a).

The Baqoroq Formation is disconformably overlain by the 364-m-thick Ashin Formation, which is dominated by shale beds intercalated with thin sandstone, calcareous siltstone and fossiliferous limestone (Fig. 4). The upper part of this formation in the studied section has been tectonically truncated. Limestone and shale beds are fossiliferous and contain remains of, for example, ammonoids, bivalves and crinoids, suggesting a Ladinian–?Early Carnian age (Tozer, 1972; Vaziri and Fürsich, 2007; Balini et al., 2009). Sedimentary structures characteristic for Bouma sequences (Bouma, 1962) and *Nereites* ichnofacies suggest that the Ashin Formation was deposited by distal turbidity currents (Hashemi Azizi et al., 2018a). Petrographic analysis of thin sections showed the Ashin Formation sandstones contain chiefly K-feldspar and volcanic

detritus as well as some fossil fragments (Hashemi Azizi et al., 2018a). The average total quartz–feldspar–lithic fragment ratio is Qt35:F46.5:L18.5 (Hashemi Azizi et al., 2018a).

Hashemi Azizi et al. (2018b) described detrital chrome spinel from the Nakhlak Group sandstones. The chemical composition of the detrital chrome spinels suggests a magmatic source. They were formed both within oceanic (mainly harzburgitic) mantle and in a supra-subduction zone (SSZ) tectonic setting. The data suggest that mafic–ultramafic rock assemblages with SSZ signatures were generated in the Palaeotethyan (or in an older oceanic) realm before their obduction as an ophiolite in pre-Late Olenekian time (Hashemi Azizi et al., 2018b).

The Triassic mixed siliciclastic, volcanoclastic and carbonate succession of the Nakhlak Group shows almost no lithological similarity with coeval rocks throughout Iran, except for the Aghdarband succession in the Kopeh-Dagh region in NE Iran (Fig. 2). Taking into account the lithological and biostratigraphical resemblances of these two successions leads to the hypothesis that both were deposited in close association at the southern Eurasian margin during the Triassic Period (e.g., Davoudzadeh et al., 1981; Baud and Stampfli; 1989; Baud et al. 1991; Ruttner, 1984, 1991, 1993; Şengör, 1990; Alavi et al. 1997). Vaziri (2011) studied in detail the ammonoid fauna. He concluded that ammonoids from the Alam Formation are similar to fauna in the Aghdarband succession and belong to a biogeographical province at the southern margin of Eurasia within the Palaeotethyan realm. Balini et al. (2019) suggested that due to the different faunal associations found in the Olenekian at Aghdarband this basin had no direct connection with the Nakhlak basin, which was probably located in a different depositional region with respect to the Triassic magmatic arc system (see also Balini et al., 2009). It has been suggested that the present position of the Nakhlak Group is probably due to the counter clockwise rotation of the CEIM and its lateral movement to the present position since the Triassic, after its formation at the southern Eurasian margin (Seyed-Emami, 1971, 2003; Davoudzadeh et al., 1981; Krystyn and Tatzreiter, 1991; Soffel and Förster, 1984; Ruttner, 1993; Soffel et al., 1996; Alavi et al., 1997; Saidi et al., 1997). To unravel the origin and palaeotectonic position of the Nakhlak Group during the Triassic, detrital zircon grains were analyzed by U–Pb geochronology.

### **3. Samples and methods**

Samples were taken from fine- to medium-grained sandstone beds from outcrop in logged sections. Lithology, stratigraphy and geographic coordinates of the studied samples are given in Table 1. The stratigraphic position of each sample is indicated in Figures 3 and 4. Sample preparation was done at the laboratories of the Geoscience Center of the University of Göttingen. After rock crushing and dry-sieving to obtain the 63–125 µm fractions, the sample material was treated with 5% cold acetic acid to remove the carbonate component if present. The heavy mineral fractions were separated using sodium polytungstate with a density of 2.85 g/mL. Zircon selection from the heavy fractions was achieved by hand-picking under a binocular microscope. Zircon grains were fixed in epoxy resin mounts and polished to expose the interior of the grains. Prior to the analyses, transmitted light photomicrographs were taken with a polarizing microscope (Zeiss Axioplan 2) equipped with a camera system to study the zircon shape and roundness. The zircon grains were classified into three groups: euhedral (well-

defined edges and angles), subhedral (slightly rounded), and anhedral (rounded) (Fig. 4). Cathodoluminescence (CL) imaging was applied using a JEOL JXA 8900 RL electron probe microanalyzer (EPMA) equipped with a CL detector (Department of Geochemistry, Geoscience Center, University of Göttingen) to reveal the internal structures (e.g., growth zones) and to guide spot placement in the zircon grains (Fig. 5).

The U–Pb age determination was performed on a sector-field ICP-MS (Element2, ThermoFisher) coupled to a 193-nm Analyte G2 Excimer Laser Ablation System (Institute of Mineralogy, University of Münster). Isotope analysis was done following the procedure described in Löwen et al. (2017). A summary of the Laser ablation ICP-MS operation parameters is given as Supplementary material (see Appendix A).

Data reduction was done following the procedure described by Kooijman et al. (2012). The data were filtered following the procedure described in Löwen et al. (2017). Histograms and kernel density estimates (KDE) plots (Fig. 6) were produced using the DensityPlotter software by Vermeesch (2012). TuffZirc age plots (Fig. 7) were produced with the Microsoft Excel add-in Isoplot (Ludwig, 2003). The international chronostratigraphic chart of Cohen et al. (2018) was used as stratigraphic reference for data interpretation.

## 4. Results

The majority of the detrital zircons from the six sandstone samples of the Triassic Nakhlak Group are clear or translucent. With the exception of the samples from the Baqoroq Formation, euhedral and subhedral grains are dominant (Fig. 4). In total, 478 zircon ages have been obtained of which 446 ages (93% of all zircons) are 90–110% concordant (Table 1). The full set of analytical data is given as Supplementary material (see Appendix A).

### 4.1. Alam Formation

In total, 163 zircon ages from two sandstone samples of the Alam Formation have been obtained, of which 149 have been used for interpretation (Table 1). The zircon grains are mainly euhedral and subhedral, with the younger sample also showing a few anhedral grains (Fig. 4). CL images reveal magmatic oscillatory zoning (Fig. 5). Samples AN12H and AN278H show similar zircon spectra, with 82–83% of all grains yielding Permian–Triassic ages (Fig. 6a,b). Older Palaeozoic zircon grains are very minor present (15–16%); Precambrian zircon grains are almost absent (Fig. 6a,b). The youngest concordant zircon grains have ages of  $243 \pm 15$  Ma in sample AN12H and  $248 \pm 6$  Ma in sample AN278H (Table 1), giving maximum ages of deposition for the Alam Formation samples. The weighted average age of the youngest coherent zircon population is  $244.7 (+0.7/-1.6)$  Ma in sample AN12H and  $248.9 (+0.3/-1.4)$  Ma in sample AN278H, using the TuffZirc algorithm of Ludwig and Mundil (2002) implemented in Isoplot (Ludwig, 2003) (Fig. 7a,b).

### 4.2. Baqoroq Formation

In total, 148 zircon ages from two sandstone samples of the Baqoroq Formation have been obtained, of which 141 have been used for interpretation (Table 1). The zircon grains in sample

BH2 are subhedral and anhedral, and only 18% are euhedral (Fig. 4). In sample BH2, the zircon grains are anhedral and minor subhedral (Fig. 4). CL images reveal magmatic oscillatory zoning in the Late Palaeozoic zircons (Fig. 5). Some grains show Neoproterozoic-aged cores overgrown by magmatic oscillatory zones of Carboniferous age (Fig. 5). Samples BH2 and BH11 show different zircon spectra (Fig. 6a,b). About 29% of all grains in BH2 have Permian–Triassic ages, 61% have older Palaeozoic ages, and 11% are of Precambrian age. In sample BH11, 5% of all zircon grains have Permian–Triassic ages, 28% have older Palaeozoic ages, and 67% are of Precambrian age. The two major Precambrian age populations are at 800–1100 Ma and 1800–2200 Ma (Fig. 6d). The youngest concordant zircon grains have ages of  $242 \pm 7$  Ma in sample BH2 and  $256 \pm 7$  Ma in sample BH11 (Table 1), giving maximum ages of deposition for the Baqoroq Formation samples. The weighted average age of the youngest coherent zircon population is  $254.7 (+2.5/-11.8)$  in sample BH2 (Fig. 7c). No average age could be calculated for the youngest coherent zircon population in sample BH11, as the required number ( $n \geq 5$ ) of ages for the TuffZirc algorithm was not available. However, an average age of  $978.2 (+22.1/-32.8)$  Ma was calculated for a coherent group of early Neoproterozoic–late Mesoproterozoic zircon grains (Fig. 7d).

#### 4.3. Ashin Formation

In total, 167 zircon ages from two sandstone samples of the Ashin Formation have been obtained, of which 156 have been used for interpretation (Table 1). The zircon grains in sample AS16H are euhedral and minor subhedral whereas in sample AS112H they are anhedral and minor subhedral, and only 5% are euhedral (Fig. 4). CL images reveal magmatic oscillatory zoning (Fig. 5). Samples AS16H and AS112H show similar zircon spectra, with 89–100% of all grains yielding Permian–Triassic ages (Fig. 6e,f). In addition, sample AS112H has a few older Palaeozoic (Devonian) zircon grains (7%); Precambrian zircon grains are almost absent (4%) (Fig. 6f). The youngest concordant zircon grains have ages of  $239 \pm 5$  Ma in sample AS16H and  $238 \pm 4$  Ma in sample AS112H (Table 1), giving maximum ages of deposition for the Ashin Formation samples. The weighted average age of the youngest coherent zircon population is  $241.3 (+0.6/-2)$  Ma in sample AS16H and  $239.6 (+0.7/-1.4)$  Ma in sample AS112H (Fig. 7e,f).

## 5. Discussion

### 5.1. Zircon morphology

In the analyzed samples from the Triassic Nakhlak Group of Central Iran, the morphology of most of the zircon grains is typical for an igneous origin. This is confirmed by CL images, as most of the zircon grains show distinct oscillatory (magmatic) zoning. Euhedral and subhedral zircon grains are prominent in the Alam Formation (Fig. 4). Higher up in the succession the zircon grains become more rounded which is well illustrated in the Baqoroq Formation (Fig. 4). This increase in rounded grains correlates with an increase in the amount of zircon grains with Neoproterozoic and Palaeoproterozoic ages, which reflects a prominent sedimentary influx of old recycled material in the Baqoroq Formation. Euhedral and subhedral zircon grains are again prominent in the lower part of the Ashin Formation. However, higher up in this formation the

zircon grains become more rounded, although the zircon ages remain similar to the lower part of the succession. This suggests a more prolonged sediment transport from source to sink as a proximal source is unlikely to produce subhedral to rounded grains over a short transport distance. An alternative scenario would be long-term grain movement in a foreshore environment and later redeposition in the offshore environment of the upper Ashin Formation. If the latter is the case, recycling from underlying strata such as the Alam Formation is possible.

## 5.2. Zircon U–Pb ages

In most samples from the Triassic Nakhlak Group, the zircon populations are similar showing a prominent Permian–Triassic age group, the only differences being due to variations in the relative abundance of early Palaeozoic and Precambrian age groups (Figs. 6 and 8). The latter age groups are ubiquitous in the Baqoroq Formation (Fig. 6c,d).

The Permian–Triassic (mainly 240–280 Ma; Fig. 8) age group represents magmatic events due to northward subduction of Palaeotethys under the southern Eurasian margin which led to the formation of a large, long-lived magmatic arc system named Silk Road Arc by Natal'in and Şengör (2005) (Figs. 1 and 9). For simplification, we use this term to refer to a Permian–Triassic magmatic arc provenance, as we cannot pinpoint to an individual magmatic rock unit as sediment source because large-scale strike-slip tectonics after arc formation complicates palaeo-tectonic reconstructions along the southern Eurasian margin (see Ruttner, 1993; Natal'in and Şengör, 2005). For example, magmatic and volcano-sedimentary rocks of this arc are found to the east of the Caspian Basin in the Turan domain (e.g., Garzanti and Gaetani, 2002; Natal'in and Şengör, 2005; Zanchetta et al., 2013, and references therein). Pre-Permian Palaeozoic magmatic rocks have also been described from this region and make up the foundation (i.e. basement) on which the arc developed (e.g., Natal'in and Şengör, 2005; Zanchetta et al., 2013, and references therein). These rocks or their recycled products during Permian–Triassic magma generation, i.e. xenocrystic zircon, represent possible sources for the pre-Permian Palaeozoic zircon grains found in the Nakhlak Group sandstones (Fig. 8).

During the time of deposition of the Baqoroq Formation, the Silk Road Arc zircon source was almost shut off. The provenance changed throughout the Baqoroq Formation (Fig. 6c,d). The lower part shows influx from the Silk Road Arc, but reduced as only 29% of all analyzed grains in sample BH2 and only 5% in sample BH11 yielded Permian–Triassic ages compared to over 80% in samples from the Alam and Ashin formations (Fig. 6). Instead, the Baqoroq Formation contains high amounts of older Palaeozoic and Precambrian zircon grains, with an increase of such grains toward the younger part of the Baqoroq Formation. The two major Precambrian age populations are at 800–1100 Ma and 1800–2200 Ma (Fig. 6d). This together with late Neoproterozoic zircon grains point toward a source region with northeast Gondwanan affinity (e.g., Meinhold et al., 2013, and references therein), as described, for example, from upper Neoproterozoic and Palaeozoic sandstones of the Alborz Mountains in northern Iran, which represent continental margin sediments of the Iranian Cimmerian blocks (Horton et al., 2008; Honarmand et al., 2016; Moghadam et al., 2017).

The change in provenance within the middle part of the Nakhlak Group is accompanied by a change in depositional environment. The Baqoroq Formation comprises continental deposits whereas the Alam and Ashin formations are made up of marine deposits

(Davoudzadeh and Seyed-Emami, 1972; Alavi et al., 1997; Seyed-Emami, 2003; Vaziri and Fürsich, 2007; Balini et al., 2009; Zanchi et al., 2009b; Hashemi Azizi et al., 2018a,b). This short-lived change in depositional environment and provenance point toward a local synsedimentary tectonic event at the southern Eurasian margin supplying detritus with a northeast Gondwanan affinity. It might indicate recycling of Cimmerian continental fragments including related platform sediments during the Middle Triassic. This seems to be supported by the observation in the Yazd block where the Cimmerian passive margin succession has been eroded down to the Lower Palaeozoic during the Middle to Late Triassic, representing flexural bulge erosion (Bagheri and Stampfli, 2008). The flexural bulge formation was likely due to the onset of collision of the northern Cimmerian margin and the accretionary wedge. Cimmerian passive margin sediments could have been incorporated in the accretionary wedge (Fig. 9c,d). Back-rotation of imbricate thrust sheets, underplating (e.g., Platt; 1986; Dorobek, 2008) and/or backthrusting in the accretionary wedge similar to that in the modern Sunda–Banda arc system in Indonesia (e.g., Silver and Reed, 1988) might have taken place and allowed uplift of metamorphosed rocks, some likely with Cimmerian affinity, providing detritus to the fore-arc basin.

Thin-section petrography confirms a metamorphic provenance, mainly metapsammite/metafelsite grains rank 2 and 3, according to the Garzanti and Vezzoli (2003) classification, composed of quartz-sericite and quartz-mica (muscovite) lithic fragments (Hashemi Azizi et al., 2018a). Alavi et al. (1997) also described metamorphic rock fragments such as quartzite, slate, gneiss and amphibolite from the Baqoroq Formation (see also Balini et al., 2009). The quartzo-lithic metamorphiclastic composition of the Baqoroq Formation reveals rapid erosion of a metamorphic complex, i.e. 'Recycled Orogen Provenance' of Dickinson (1985) and 'Axial Belt Provenance' of Garzanti et al. (2007), respectively (Zanchi et al., 2009b). Also, such a provenance signature may characterize first-cycle detritus from metamorphic basement rocks representing remnants of the continental margins caught in collision, as well as polycyclic detritus recycled from orogen-derived clastic wedges accreted along the mountain front (Garzanti et al., 2007, and references therein).

A likely source for metamorphic rocks of the Baqoroq Formation could be the Anarak Metamorphic Complex in the Anarak region (Fig. 2), ca. 20 km to the south of Nakhlak which represents the remnant of a Variscan accretionary wedge (Bagheri and Stampfli 2008; Zanchi et al., 2009b, 2015; Buchs et al., 2013). Although zircon data are limited to a few analysis only, magmatic rocks show Early Permian ( $291.1 \pm 1.8$  Ma; Zanchi et al., 2015) and Late Permian ( $262.3 \pm 1.0$  Ma; Bagheri and Stampfli, 2008) ages, and xenocrystic zircon grains yielded single ages from  $953.6 \pm 8.2$  to  $456.6 \pm 4.3$  Ma which can be roughly grouped into clusters of Tonian ( $953.6 \pm 8.2$  Ma), Cryogenian (three spots:  $702.7 \pm 6.1$  to  $642.6 \pm 4.1$  Ma), Ediacaran (four spots:  $621.7 \pm 5.6$  to  $576.2 \pm 4.4$  Ma), Early ( $481.6 \pm 3$  and  $478.8 \pm 2.2$  Ma) and Late Ordovician ( $457.1 \pm 3$ ) ages (Zanchi et al., 2015). These ages are similar to pre-Permian ages found in the Baqoroq Formation sandstones (Figs. 6 and 8).

We speculate that the short-lived changes in provenance and depositional environment observed in the Nakhlak Group might be related to short-lived changes in the type, geometry and deformation manner of the fore-arc basin, i.e. nonaccretionary (erosional) type to neutral or compressional accretionary type, following the definitions by Noda (2016). Strike-slip

tectonics probably played an important role for the geodynamics during the Triassic (see Ruttner, 1993; Natal'in and Şengör, 2005).

The collisional event of the Cimmerian blocks with the Eurasian margin that led to the closure of Palaeotethys has been called the Eo-Cimmerian (or Eocimmerian) Orogeny (e.g., Şengör, 1984) and is commonly thought to have taken place in the Late Triassic (e.g., Şengör, 1979, 1984; Berberian and King, 1981; Şengör et al., 1988; Stampfli and Kozur, 2006; Wilmsen et al., 2009; Zanchi et al., 2009a).

Two scenarios are possible based on our U–Pb detrital zircon geochronological evidence from the Triassic of Central Iran. Continental fragments with a northeast Gondwanan affinity were accreted at the southern Eurasian margin during the Late Palaeozoic (e.g., Bagheri and Stampfli, 2008; Zanchi et al., 2015) and later recycled during the Triassic.

Alternatively, besides scenario 1, Cimmerian continental blocks and related sediments, similar to the upper Neoproterozoic and Palaeozoic sandstones of the Alborz Mountains in northern Iran, which show detrital zircon ages with northeast Gondwanan affinity (Horton et al., 2008; Honarmand et al., 2016; Moghadam et al., 2017), were incorporated in the accretionary wedge at the southern Eurasian margin during the Middle Triassic (Fig. 9c). The rocks were metamorphosed, and parts of those were uplifted and prone to erosion supplying detrital material with a northeast Gondwanan (Cimmerian) provenance to the fore-arc basin in pre-Late Triassic time. Subsidence analysis of Triassic sediments from the Alborz Mountains, i.e. the northern passive margin of Cimmeria, seem to confirm a pre-Late Triassic age for the collision of the Iranian Cimmerian blocks with Eurasia, to which a Ladinian age has been assigned (Saidi et al., 1997). Thus, according to that and the detrital zircon data from the Baqoroq Formation (this study), the harbinger of the Eo-Cimmerian orogeny in Iran probably occurred during late Middle Triassic (Middle Ladinian) times.

After deposition of the continental Baqoroq Formation, the depositional basin rapidly subsided to become deep marine as indicated by the *Nereites* ichnofacies in the Ashin Formation (Vaziri and Fürsich, 2007). The rapid subsidence was probably triggered by strike-slip tectonics due to oblique convergence of the subducting Palaeotethys (e.g., Natal'in and Şengör, 2005). In the lower part of the Ashin Formation, the majority of the Permian–Triassic-aged zircon grains are euhedral and minor subhedral (Fig. 4), pointing toward a proximal source. In the upper part of the Ashin Formation, the amount of proximal arc material was reduced, as Permian–Triassic-aged zircon grains are subhedral and anhedral (rounded). Thus, a provenance change can be recognized throughout the Ladinian–?Early Carnian, with a more distal source area or supply of recycled sediment to the younger part of the Ashin Formation, probably derived from an intra-arc or a back-arc region. This may be the time when subduction gradually stopped, probably associated with slab break-off of the subducting Palaeotethys slab, leading to the cessation of arc magmatism during the Late Triassic (Alavi et al., 1997) (Fig. 9d).

## 6. Conclusion

The new zircon U–Pb geochronological data from the Triassic Nakhlak Group sandstones of Central Iran show a prominent Permian–Triassic age group, the only differences being due to variations in the relative abundance of early Palaeozoic and Precambrian age groups (e.g., ca. 550–1100 Ma and ca. 1800–2200 Ma). The latter age groups are ubiquitous in the middle part

of the Nakhlak Group, i.e. ?Upper Anisian–Middle Ladinian Baqoroq Formation, and point toward a source region with a northeast Gondwanan affinity.

Overall, our data provide univocal evidence for a sediment source from the southern Eurasian active margin (related to the Silk Road Arc) and a short-lived northeast Gondwana-derived provenance during the late Middle Triassic. The latter indicates a pre-Late Triassic arrival of northeast Gondwana-derived continental fragments at the southern Eurasian margin. The northeast Gondwanan source was probably derived from the Cimmerian blocks *sensu stricto*. It may be seen as the harbinger of the Eo-Cimmerian orogeny in Iran that was underway during late Middle Triassic (Middle Ladinian) times, earlier than previously thought.

### **Acknowledgements**

The first author gratefully acknowledges the support of the German Academic Exchange Service (DAAD). The Geoscience Center of the University of Göttingen is thanked for providing access to laboratory facilities for sample preparation. We thank Andreas Kronz for providing access to the electron microprobe for CL imaging, Beate Schmitte for assistance at the LA-ICP-MS facility, Gérard M. Stampfli for his pre-submission remarks, and the anonymous reviewers for constructive and thorough comments.

### **Appendix A. Supplementary material**

Supplementary material related to this article can be found online at xxxxxx

### **References**

- Alavi, M., Vaziri, H., Seyed Emami, K., Lasemi, Y., 1997. The Triassic and associated rocks of the Nakhlak and Aghdarband areas in central and northeastern Iran as remnants of the southern Turanian active continental margin. *Geological Society of America Bulletin* 109, 1563–1575.
- Amante, C., Eakins, B.W., 2009. ETOPO1 1 Arc-Minute Global Relief Model: Procedures, Data Sources and Analysis. NOAA Technical Memorandum NESDIS NGDC-24. National Geophysical Data Center, NOAA, <https://doi.org/10.7289/V5C8276M> [last accessed 3 July 2019]
- Bagheri, S., Stampfli, G.M., 2008. The Anarak, Jandaq and Posht-e-Badam metamorphic complexes in Central Iran: new geological data, relationships and tectonic implications. *Tectonophysics* 451, 123–155.
- Balini, M., Nicora, A., Berra, F., Garzanti, F., Levera, M., Mattei, M., Muttoni, M., Zanchi, A., Bollati, I., Larghi, C., Zanchetta, S., Salamati, R., Mossavvari, F., 2009. The Triassic stratigraphic succession of Nakhlak (Central Iran), a record from an active margin. In: Brunet, M.F., Wilmsen, M., Granath, J.W. (Eds.), *South Caspian to Central Iran Basins*. Geological Society London, Special Publication 312, 287–321.
- Balini, M., Nicora, A., Zanchetta, S., Zanchi, A., Marchesi, R., Vuolo, I., Hosseiniyoon, M., Norouzi, M., Soleimani, S., 2019. Olenekian to early Ladinian stratigraphy of the western part of the Aghdarband window (Kopeh-Dag, NE Iran). *Rivista Italiana di Palaeontologia e Stratigrafia* 125, 283–315.

- Baud, A. Stampfli, G.M., 1989. Tectonogenesis and evolution of a segment of the Cimmerides: The volcano-sedimentary Triassic of Aghdarband (Kopet-Dagh, North-East Iran). In: Şengör, A.M.C. (Eds.), *Tectonic Evolution of the Tethyan region*. Kluwer, 265–275.
- Baud, A., Stampfli, G., Steen, D., 1991. The Triassic Aghdarband Group: volcanism and geological evolution. *Abhandlungen der Geologischen Bundesanstalt Wien* 38, 125–137.
- Berberian, M., King, G., 1981. Toward a paleogeographic and tectonic evolution of Iran. *Canadian Journal of Earth Sciences* 18, 210–265.
- Berra, F., Balini, M., Levera, M., Nicora, A., Salamati, R., 2012. Anatomy of carbonate mounds from the Middle Anisian of Nakhlak (Central Iran): architecture and age of a subtidal microbial-bioclastic carbonate factory. *Facies* 58, 685–705.
- Bouma, A.H., 1962. *Sedimentology of some flysch deposits: a graphic approach to facies interpretation*. Amsterdam, Elsevier, 168 pp.
- Buchs, D.M., Bagheri, S., Martin, L., Hermann, J., Arculus, R., 2013. Paleozoic to Triassic ocean opening and closure preserved in Central Iran: constraints from the geochemistry of meta-igneous rocks of the Anarak area. *Lithos* 172–173, 267–287.
- Cohen, K.M., Harper, D.A.T., Gibbard, P.L., Fan, J.-X., 2018. The International Chronostratigraphic Chart. International Commission on Stratigraphy, <http://www.stratigraphy.org/ICSchart/ChronostratChart2018-08.pdf>
- Davoudzadeh, M., Seyed-Emami, K., 1972. Stratigraphy of the Triassic Nakhlak Group, Anarak region, Central Iran. *Geological Survey of Iran Report* 28, 5–28.
- Davoudzadeh, M., Soffel, H., Schmidt, K., 1981. On the rotation of Central–East-Iran microplate. *Neues Jahrbuch für Geologie und Paläontologie, Monatshefte* 3, 180–192.
- Dickinson, W.R., 1985. Interpreting provenance relations from detrital modes of sandstones. In: Zuffa, G.G. (Ed.), *Provenance of Arenites*. Reidel, Dordrecht NATO ASI Series 148, 333–361.
- Dorobek, S.L., 2008. Carbonate-platform facies in volcanic-arc settings: Characteristics and controls on deposition and stratigraphic development. In: Draut, A., Clift, P.D., Scholl, D.W. (Eds.), *Formation and applications of the sedimentary record in arc collision zones*. Geological Society of America, Special Paper 436, 55–90.
- Garzanti, E., Gaetani, M., 2002. Unroofing history of Late Paleozoic magmatic arcs within the “Turan Plate” (Tuarkyr, Turkmenistan). *Sedimentary Geology* 151, 67–87.
- Garzanti, E., Vezzoli, G., 2003. A classification of metamorphic grains in sands based on their composition and grade. *Journal of Sedimentary Research* 73, 830–837.
- Garzanti, E., Doglioni, C., Vezzoli, G., Andò, S. 2007. Orogenic belts and orogenic sediment provenance. *Journal of Geology* 115, 315–334.
- Hashemi Azizi, S.H., Rezaee, P., Jafarzadeh, M., Meinhold, G., Moussavi Harami, S.R., Masoodi, M., 2018a. Early Mesozoic sedimentary–tectonic evolution of the Central-East Iranian Microcontinent: Evidence from a provenance study of the Nakhlak Group. *Geochemistry* 78, 340–355.
- Hashemi Azizi, S.H., Rezaee, P., Jafarzadeh, M., Meinhold, G., Moussavi Harami, S.R., Masoodi, M., 2018b. Evidence from detrital chrome spinel chemistry for a Paleo-Tethyan intra-oceanic island-arc provenance recorded in Triassic sandstones of the Nakhlak Group, Central Iran. *Journal of African Earth Sciences* 143, 242–252.
- Honarmand, M., Li, X.-H., Nabatian, G., Rezaeian, M., Etemad-Saeed, N., 2016. Neoproterozoic–Early Cambrian tectono-magmatic evolution of the Central Iranian terrane, northern

- margin of Gondwana: Constraints from detrital zircon U–Pb and Hf–O isotope studies. *Gondwana Research* 37, 285–300.
- Horton, B.K., Hassanzadeh, J., Stockli, D.F., Axen, G.J., Gillis, R.J., Guest, B., Amini, A., Fakhari, M.D., Zamanzadeh, S.M., Grove, M., 2008. Detrital zircon provenance of Neoproterozoic to Cenozoic deposits in Iran: implications for chronostratigraphy and collisional tectonics. *Tectonophysics* 451, 97–122.
- Kooijman, E., Berndt, J., Mezger, K., 2012. U–Pb dating of zircon by laser ablation ICP-MS: recent improvements and new insights. *European Journal of Mineralogy* 24, 5–21.
- Krystyn, L., Tatzreiter, F., 1991. Middle Triassic ammonoids from Aghdarband (NE-Iran) and their paleobiogeographical significance. *Abhandlungen der Geologischen Bundesanstalt* 38, 139–163.
- Löwen, K., Meinhold, G., Güngör, T., Berndt, J., 2017. Palaeotethys-related sediments of the Karaburun Peninsula, western Turkey: constraints on provenance and stratigraphy from detrital zircon geochronology. *International Journal of Earth Sciences* 106, 2771–2796.
- Ludwig, K., 2003. *Isoplot/Ex 3.00. A geochronological toolkit for Microsoft Excel*. Berkeley Geochronology Center, Special Publication 4, 1–70.
- Ludwig, K.R., Mundil, R., 2002. Extracting reliable U–Pb ages and errors from complex populations of zircons from Phanerozoic tuffs. *Geochemica et Cosmochimica Acta* 66 (Supplement 1), 461.
- Meinhold, G., Morton, A.C., Avigad, D., 2013. New insights into peri-Gondwana paleogeography and the Gondwana super-fan system from detrital zircon U–Pb ages. *Gondwana Research* 23, 661–665.
- Meinhold, G., Morton, A.C., Fanning, C.M., Frei, D., Howard, J.P., Phillips, R.J., Strogon, D., Whitham, A.G., 2011. Evidence from detrital zircons for recycling of Mesoproterozoic and Neoproterozoic crust recorded in Paleozoic and Mesozoic sandstones of southern Libya. *Earth and Planetary Science Letters* 312, 164–175.
- Moghadam, H., Li, X.-H., Griffin, W.L., Stern, R.J., Thomsen, T.B., Meinhold, G., Aharipour, R., O'Reilly, S.Y., 2017. Early Paleozoic tectonic reconstruction of Iran: Tales from detrital zircon geochronology. *Lithos* 268–271, 87–101.
- Muttoni, G., Gaetani, M., Kent, D.V., Sciunnach, D., Angiolini, L., Berra, F., Garzanti, E., Mattei, M., Zanchi, A., 2009a. Opening of the Neo-Tethys Ocean and the Pangea B to Pangea A transformation during the Permian. *GeoArabia* 14, 17–48.
- Muttoni, G., Mattei, M., Balini, M., Zanchi, A., Gaetani, M., Berra, F., 2009b. The drift history of Iran from the Ordovician to the Triassic. In: Brunet, M.F., Wilmsen, M., Granath, J.W. (Eds.), *South Caspian to Central Iran Basins*. Geological Society London, Special Publication 312, 7–29.
- Natal'in, B.A., Şengör, A.M.C., 2005. Late Palaeozoic to Triassic evolution of the Turan and Scythian platforms: The pre-history of the Palaeo-Tethyan closure. *Tectonophysics* 404, 175–202.
- Natal'in, B.A., Sunal, G., Gün, E., Wang, B., Zhiqing, Y., 2016. Precambrian to Early Cretaceous rocks of the Strandja Massif (northwestern Turkey): evolution of a long lasting magmatic arc. *Canadian Journal of Earth Sciences* 53, 1312–1335.
- Noda, A., 2016. Forearc basins: Types, geometries, and relationships to subduction zone dynamics. *Geological Society of America Bulletin* 128, 879–895.

- Platt, J.P., 1986. Dynamics of orogenic wedges and the uplift of high-pressure metamorphic rocks. *Geological Society of America Bulletin* 97, 1037–1053.
- Ruttner, A.W., 1984. The pre-Liassic basement of the eastern Kopet Dag Range. *Neues Jahrbuch für Geologie und Paläontologie, Abhandlungen* 168, 256–268.
- Ruttner, A.W., 1991. Geology of the Aghdarband area (Kopeh Dag). NE-Iran. *Abhandlungen der Geologischen Bundesanstalt* 38, 7–79.
- Ruttner, A.W., 1993. Southern borderland of Triassic Laurasia in north-east Iran. *Geologische Rundschau* 82, 110–120.
- Saidi, A., Brunet, M.F., Ricou, L.E., 1997. Continental accretion of the Iran Block to Eurasia as seen from Late Paleozoic to Early Cretaceous subsidence curves. *Geodynamica Acta* 10, 198–208.
- Şengör, A.M.C., 1979. Mid-Mesozoic closure of Tethys and its implications. *Nature* 279, 590–593.
- Şengör, A.M.C., 1984. The Cimmeride orogenic system and the tectonics of Eurasia. *Geological Society of America, Special Paper* 195, 1–82.
- Şengör, A.M.C., 1990. A new model for the late Palaeozoic–Mesozoic tectonic evolution of Iran and implications for Oman. In: Robertson, A.H.F., Searle, M.P., Ries, A.C. (Eds.), *The Geology and Tectonics of the Oman Region*. Geological Society London, Special Publication 49, 797–831.
- Şengör, A.M.C., Natalin, B.A., 1996. Paleotectonics of Asia: fragments of a synthesis. In: Yin, A., Harrison, T.M. (Eds.), *The Tectonic Evolution of Asia*. Cambridge University Press, pp. 486–640.
- Şengör, A.M.C., Altiner, D., Cin, A., Ustaömer, T., Hsü, K.J., 1988. Origin and assembly of the Tethyside orogenic collage at the expense of Gondwana Land. In: Audley-Charles, M.G., Hallam, A. (Eds.), *Gondwana and Tethys*. Geological Society London, Special Publication 37, 119–181.
- Seyed-Emami, K., 1971. A summary of the Triassic in Iran. *Geological Survey of Iran, Report* 20, 41–53.
- Seyed-Emami, K., 2003. Triassic of Iran. *Facies* 48, 91–106.
- Silver, E.A., Reed, D.L., 1988. Backthrusting in accretionary wedges. *Journal of Geophysical Research* 93, 3116–3126.
- Soffel, H.C., Förster, H.G., 1984. Polar Wander Path of the Central-East-Iran Microplate including new results. *Neues Jahrbuch für Geologie und Paläontologie, Abhandlungen* 168, 165–172.
- Soffel, H.C., Davoudzadeh, M., Rolf, C., Schmidt, S., 1996. New palaeomagnetic data from Central Iran and a Triassic palaeoreconstruction. *Geologische Rundschau* 85, 293–302.
- Stampfli, G.M., 2000. Tethyan oceans. In: Bozkurt, E., Winchester, J.A., Piper, J.D.A. (Eds.), *Tectonics and Magmatism in Turkey and the Surrounding Area*. Geological Society London, Special Publication 173, 1–23.
- Stampfli, G.M., Borel, G., 2002. A plate tectonic model for the Paleozoic and Mesozoic constrained by dynamic plate boundaries and restored synthetic oceanic isochrones. *Earth and Planetary Science Letters* 196, 17–33.

- Stampfli, G.M., Kozur, H., 2006. Europe from the Variscan to the Alpine cycles. In: Gee, D.G., Stephenson, R.A. (Eds.), *European lithosphere dynamics*. Geological Society, London, *Memoirs* 32, 57–82.
- Stöcklin, J., 1968. Structural history and tectonics of Iran: A review. *American Association of Petroleum Geologists, Bulletin* 52, 1229–1258.
- Tozer, E.T., 1972. Triassic ammonoids and *Daonella* from the Nakhlak Group, Anarak region, Central Iran. *Geological Survey of Iran, Report* 28, 29–69.
- Vaziri, S.H., Fürsich, F.T., 2007. Middle to Upper Triassic deep-water trace fossils from the Ashin Formation, Nakhlak Area, Central Iran. *Journal of Sciences, Islamic Republic of Iran* 18, 263–268.
- Vaziri, S.H., Senowbari-Daryan, B., Kohansal-Ghadimvand, N., 2005. Lithofacies and microfacies of the Upper Cretaceous rocks (Sadr unit) of Nakhlak area in Northeastern Iran, Central Iran. *Journal of Geosciences, Osaka City University* 48, 71–80.
- Vaziri, S.H., Fürsich, F.T., Kohansal-Ghadimvand, N., 2012. Facies analysis and depositional environments of the Upper Cretaceous Sadr unit in the Nakhlak area, Central Iran. *Revista Mexicana de Ciencias Geológicas* 29, 384–397.
- Vaziri, S.H., 2011. Sedimentary structures and depositional environment of the Ashin Formation in Nakhlak area, Central Iran. *Iranian Journal of Earth Sciences* 3, 69–79.
- Vaziri, S.H., 2012. Geological Map of Iran, Nakhlak Mine, 1:25,000. Geological Survey and Mineral Exploration of Iran.
- Vermeesch, P., 2012. On the visualisation of detrital age distributions. *Chemical Geology* 312–313, 190–194.
- Wilmsen, M., Fürsich, F.T., Seyed-Emami, K., Reza Majidifard, M., Taheri, J., 2009. The Cimmerian Orogeny in northern Iran: tectono-stratigraphic evidence from the foreland. *Terra Nova* 21, 211–218.
- Zanchetta, S., Berra, F., Zanchi, A., Bergomi, M., Caridroit, M., Nicora, M., Heidarzadeh, G., 2013. The record of the Late Palaeozoic active margin of the Palaeotethys in NE Iran: constraints on the Cimmerian orogeny. *Gondwana Research* 24, 1237–1266.
- Zanchi, A., Zanchetta, S., Berra, F., Mattei, M., Garzanti, E., Molyneux, S., Nawab, A., Sabouri, J., 2009a. The Eo-Cimmerian (Late? Triassic) orogeny in north Iran. In: Brunet, M.F., Wilmsen, M., Granath, J.W. (Eds.), *South Caspian to Central Iran Basins*. Geological Society London, *Special Publication* 312, pp. 31–55.
- Zanchi, A., Zanchetta, S., Garzanti, E., Balini, M., Berra, F., Mattei, M., Muttoni, G., 2009b. The Cimmerian evolution of the Nakhlak–Anarak area, Central Iran, and its bearing for the reconstruction of the history of the Eurasian margin. In: Brunet, M.F., Wilmsen, M., Granath, J.W. (Eds.), *South Caspian to Central Iran Basins*. Geological Society London, *Special Publication* 312, 261–286.
- Zanchi, A., Malaspina, N., Zanchetta, S., Berra, F., Benciolini, L., Bergomi, M., Cavallo, A., Javadi, H.R., Kouhpeyma, M., 2015. The Cimmerian accretionary wedge of Anarak, Central Iran. *Journal of Asian Earth Sciences* 102, 45–72.

## Figure captions

**Figure 1.** (a) Permian–Triassic palaeotectonic reconstruction (Mollweide full globe projection) of Pangaea A (modified after Muttoni et al., 2009a) showing the Cimmerian blocks with the Palaeotethys to the north and the Neotethys to the south. The Palaeotethys and Panthalassa trenches are indicated by solid triangles, the Neotethys ridge by small diverging arrows, and transcurrent plate motion by half arrows. (b) Permian–Triassic palaeotectonic reconstruction showing the position of the Silk Road Arc that evolved at the southern Eurasian margin due to the northward subduction of Palaeotethys (modified after Natal'in and Şengör, 2005). The approximate position of the study area is indicated by a black star.

**Figure 2.** Simplified map of Iran with main tectonic subdivisions (compiled and modified after Berberian and King, 1981; Zanchi et al., 2009b; Buchs et al., 2013). The study area is indicated by a black frame. The inset (topographic map after Amante and Eakins, 2009) shows the location of the study area within the Arabia–Eurasia convergence zone. AG – Aghdarband, AJT – Anarak–Jandaq terrane, AN – Anarak, CEIM – Central-East Iranian Microcontinent, BY – Bayazeh, EIR – Eastern Iran, JN – Jandaq, MS – Mashhad, PB – Posht-e-Badam, RS – Rasht, SC – south Caspian Sea basin, TA – Takab. The colour version of this figure is available in the web version of this article.

**Figure 3.** Geological map of the Nakhlak Mountain (modified after Vaziri, 2012) showing the study area. The studied sections in the Alam, Baqoroq, and Ashin formations of the Nakhlak Group are illustrated by black solid lines. The position of each sample used U–Pb zircon dating is indicated by open circles. The colour version of this figure is available in the web version of this article.

**Figure 4.** Composite lithological column for the Nakhlak Group fore-arc sedimentary succession showing the stratigraphic position of sandstone samples used for U–Pb zircon dating. Location of each of the logged sections is shown in Figure 3. The subdivision of the Baqoroq Formation in a lower and an upper part has already been recognized by Alavi et al. (1997). Here it is based on the different amount of metamorphic lithoclasts observed in thin-section petrography (Hashemi Azizi et al., 2018a). Pie charts show the qualitative analysis of grain shapes. Euhedral – well-defined edges and angles; Subhedral – slightly rounded; Anhedral – rounded.

**Figure 5.** Photomicrographs (plane-polarized light) and CL images of representative zircon grains from analyzed samples with location of the LA-ICP-MS analysis spot and corresponding  $^{206}\text{U}/^{238}\text{Pb}$  age ( $\pm 2\sigma$ ), the exception being spot AN278H-19 with corresponding  $^{207}\text{Pb}/^{206}\text{Pb}$  age ( $\pm 2\sigma$ ). Letter-number code above the ages: sample-spot. The scale bar represents 50  $\mu\text{m}$  in all images.

**Figure 6.** Histograms and kernel density estimate (KDE) plots of the detrital zircon U–Pb age spectra in samples from the Alam, Baqoroq, and Ashin formations of the Nakhlak Group, Central Iran (bin width = 100 Ma). On the right side in each diagram, percentages of Permian–Triassic, Cambrian–Carboniferous, and Precambrian zircon age groups are shown. Inlet shows close-up of the Phanerozoic age range (bin width = 25 Ma). n – number of concordant ages.

**Figure 7.** TuffZirc age plots for the youngest populations of coherent detrital zircon U–Pb ages from samples of the Alam, Baqoroq, and Ashin formations of the Nakhlak Group, Central Iran. Blue bars represent analyses rejected for the TuffZirc calculation and red bars show the coherent data used to obtain the best age estimate using the TuffZirc algorithm of Ludwig and Mundil (2002) implemented in

Isoplot (Ludwig, 2003). Although sample BH11 yielded individual Palaeozoic ages, the required minimum number of coherent ages ( $n \geq 5$ ) for the TuffZirc algorithm could only be achieved from a late Mesoproterozoic–early Neoproterozoic age population.

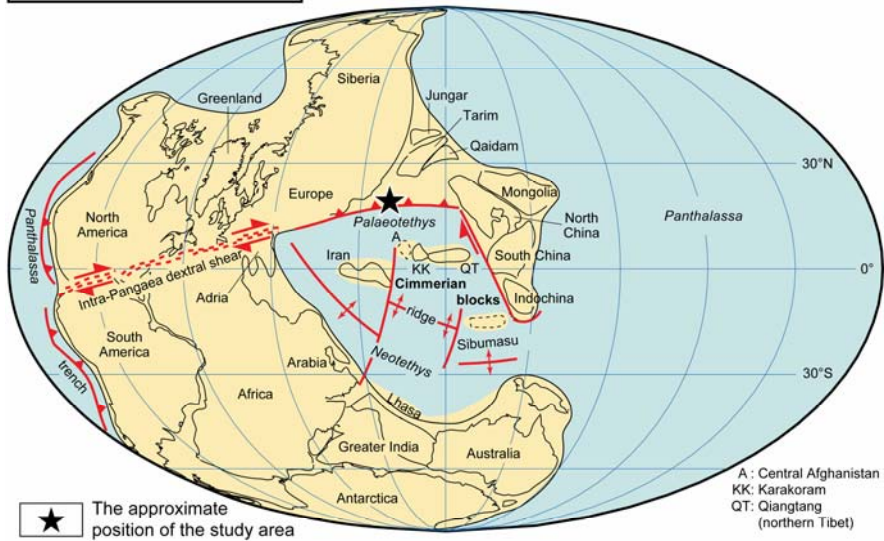
**Figure 8.** Histogram and kernel density estimate (KDE) plots show summary of U–Pb analytical detrital zircon data for all samples analyzed in this study (bin width = 100 Ma). Inlet shows close-up of the Phanerozoic age range (bin width = 25 Ma). Sediment supply from prominent source rocks/regions is indicated. n – number of concordant ages, Mes. – Mesozoic, Pal. – Palaeozoic, Neoprot. – Neoproterozoic, Mesoprot. – Mesoproterozoic, Neoar. – Neoproterozoic, Mesoar. – Mesoproterozoic, Palaeoar. – Palaeoproterozoic.

**Figure 9.** Reconstruction of the Palaeotethys, the Cimmerian blocks and the magmatic arc system at the southern Eurasian margin, i.e. Silk Road Arc (Natal'in and Şengör, 2005), during Late Permian and Triassic times, according to the palaeotectonic models of Bagheri and Stampfli (2008), Buchs et al. (2013), and taking into account the results of this study. (a) Continued subduction of oceanic lithospheric mantle and oceanic crust of Palaeotethys beneath the southern Eurasian active margin. Formation of an accretionary wedge. Relics are preserved within the Anarak Metamorphic Complex in Central Iran (e.g., Bagheri and Stampfli, 2008; Buchs et al., 2013). OIB – Oceanic island basalts. (b) Deposition of the Nakhlak Group (NG) sediments, i.e. Alam Formation, in a fore-arc basin along the southern Eurasian margin. (c) Cimmerian blocks approach the southern Eurasian margin. Passive margin sediments with NE Gondwanan provenance are incorporated in the accretionary wedge. Accretionary wedge material becomes recycled into the fore-arc basin. Time of deposition of the Baqoraq Formation. (d) Final stages of subduction and continental collision in Late Triassic time. Slab break-off of the subducting Palaeotethys slab has probably led to the cessation of arc magmatism (e.g., Alavi et al., 1997). Deposition of the Ashin Formation in late Middle and early Late Triassic times. See Section 5 for detailed explanations.

### Table caption

**Table 1.** Sample information. *First six columns* provide the location, stratigraphic position and rock type of samples analyzed in this study. Detailed stratigraphic position of samples is shown in Figure 4. Stratigraphic position is according to biostratigraphy as discussed in Hashemi Azizi et al. (2018a). Rock type is according to thin-section petrography (Hashemi Azizi et al., 2018a). Note that samples AS112H, AS16H, BH2 and AN12H correspond to samples AS112, AS16, B18 and AN94 in Hashemi Azizi et al. (2018a), respectively. *Last four columns* provide a summary of detrital zircon ages of samples analyzed in this study. U–Pb ages in the last column are given with 2-sigma uncertainties. The full data set is given as Supplementary material (see Appendix A).

**(a) Permian–Triassic**



**(b) Permian–Triassic**

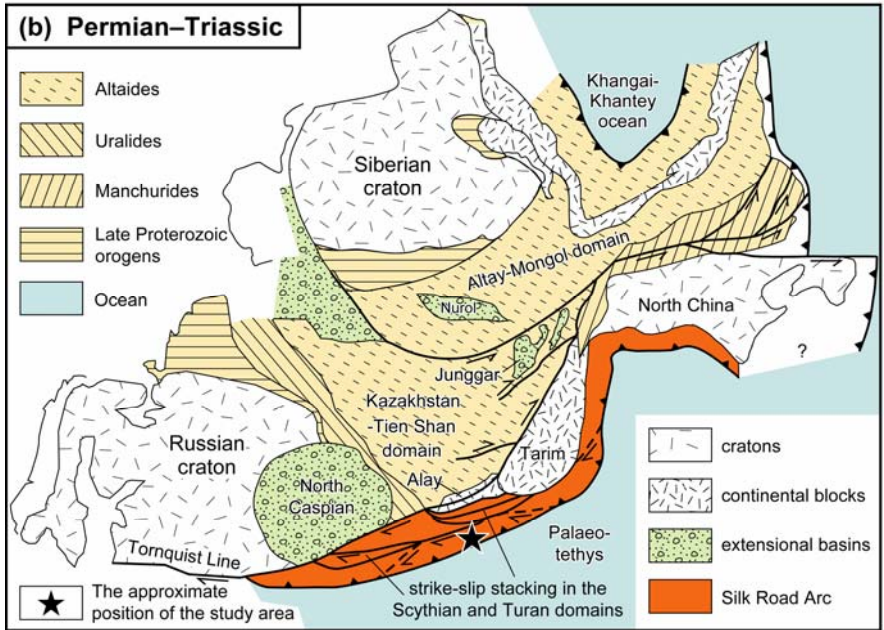


**Figure 1**

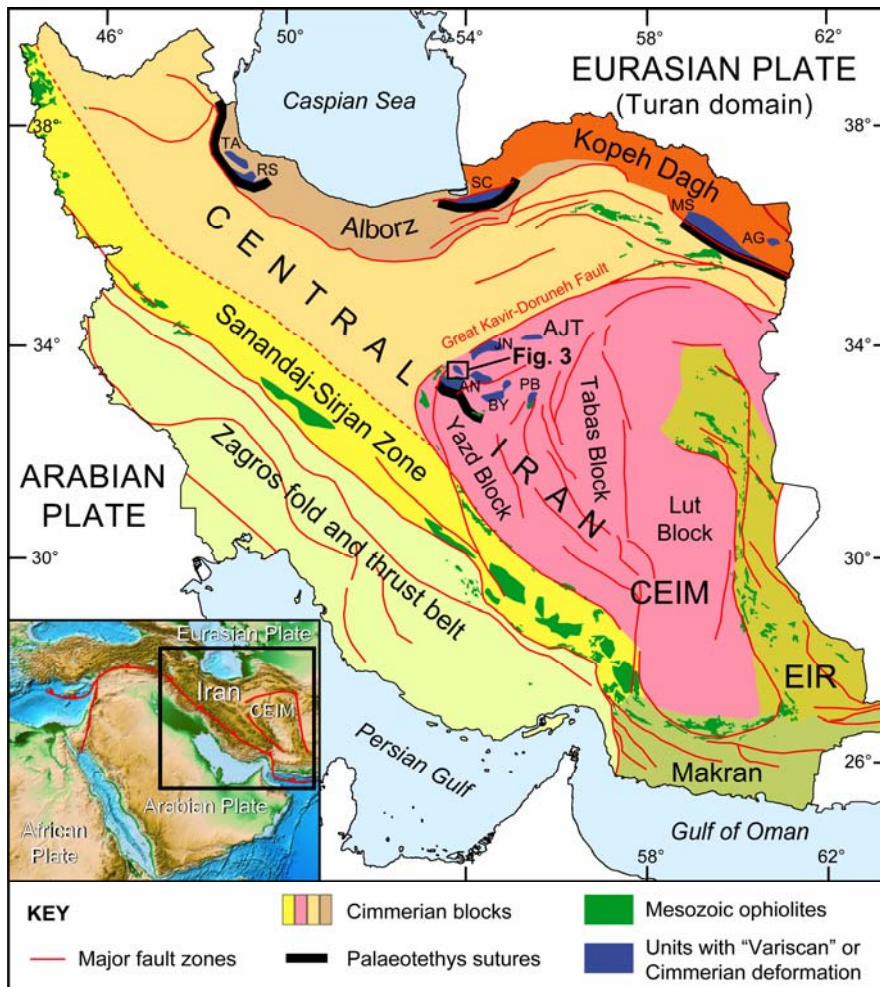
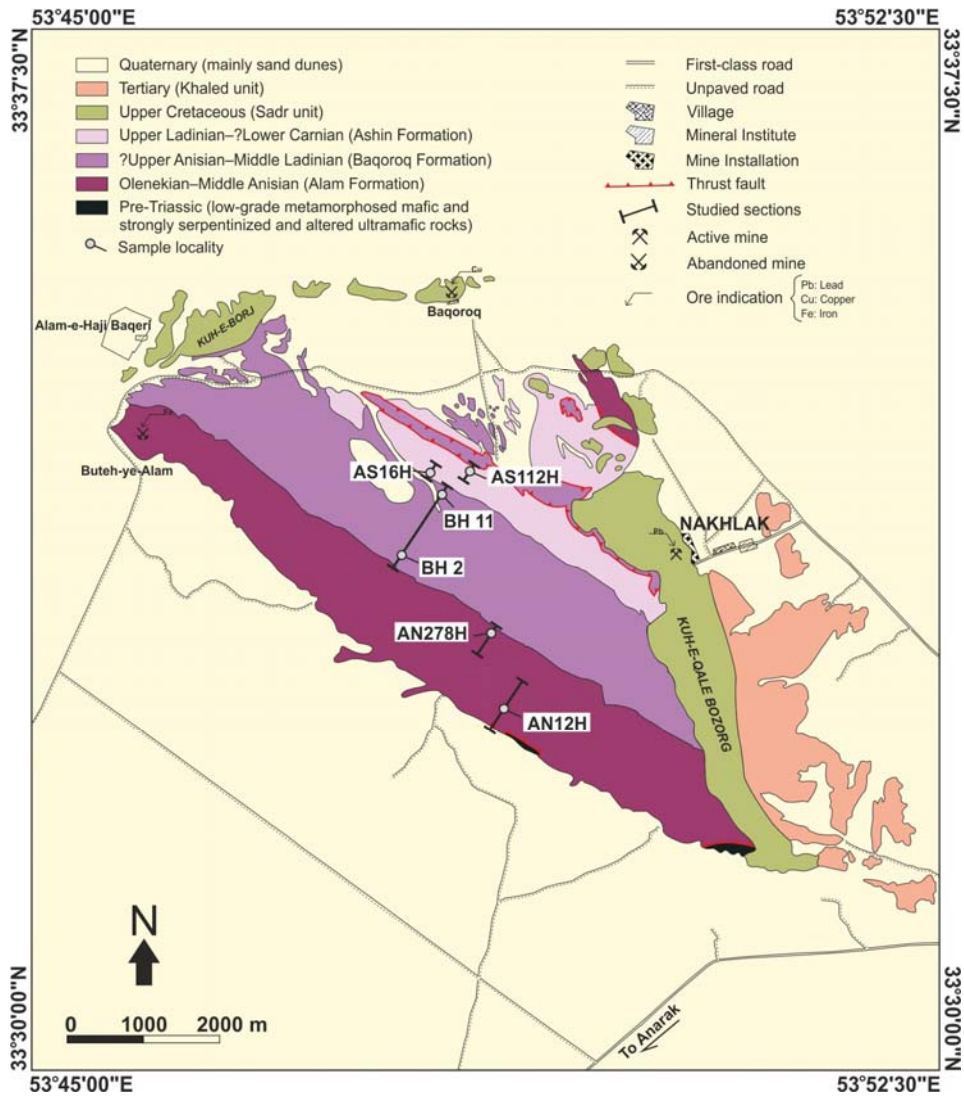


Figure 2



**Figure 3**

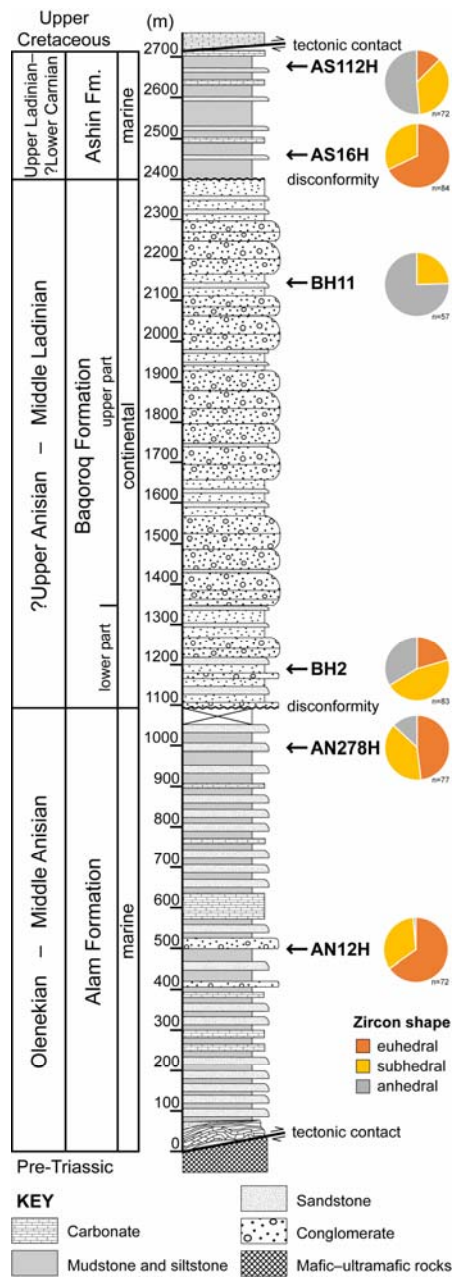


Figure 4



Figure 5

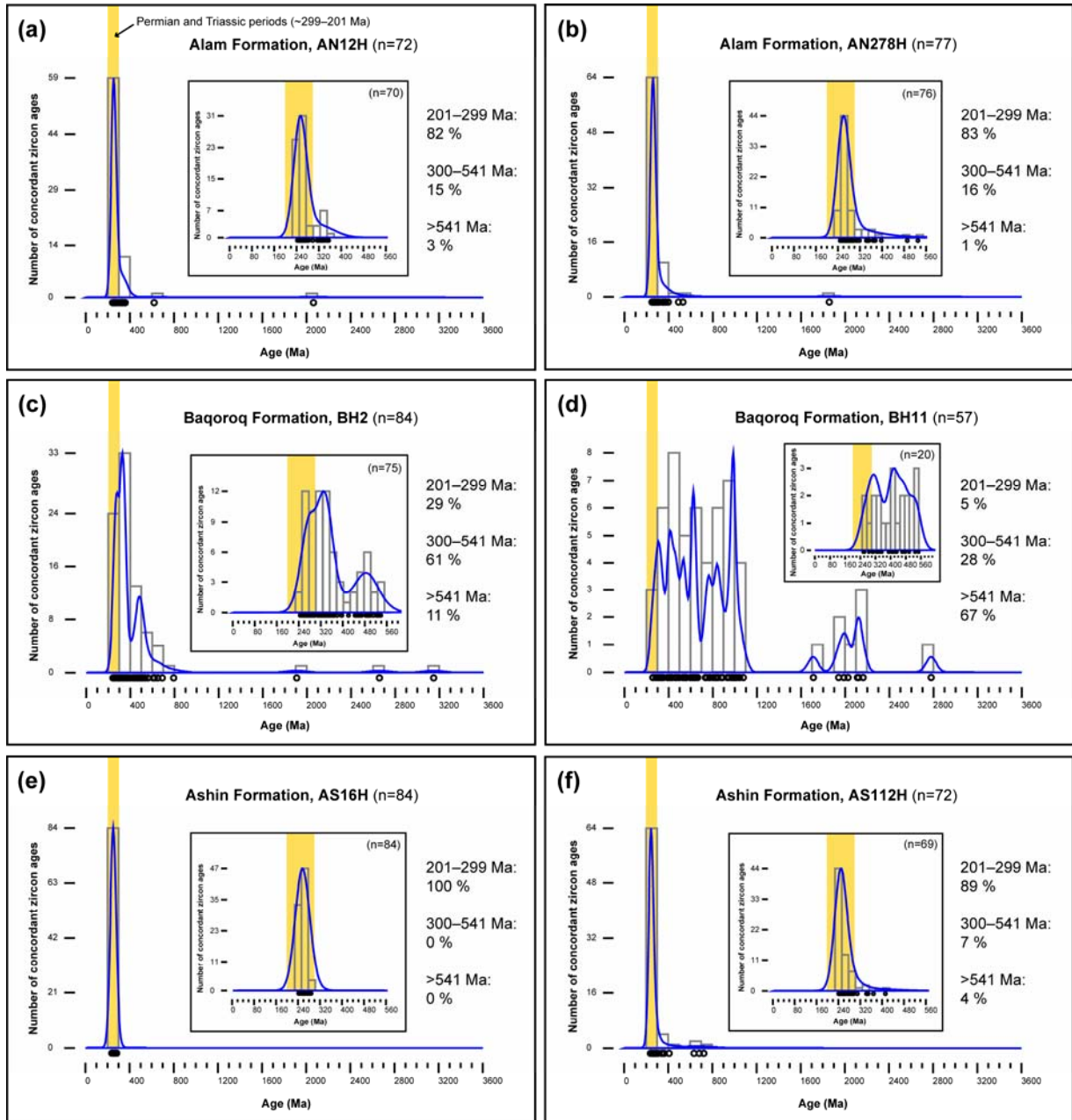


Figure 6

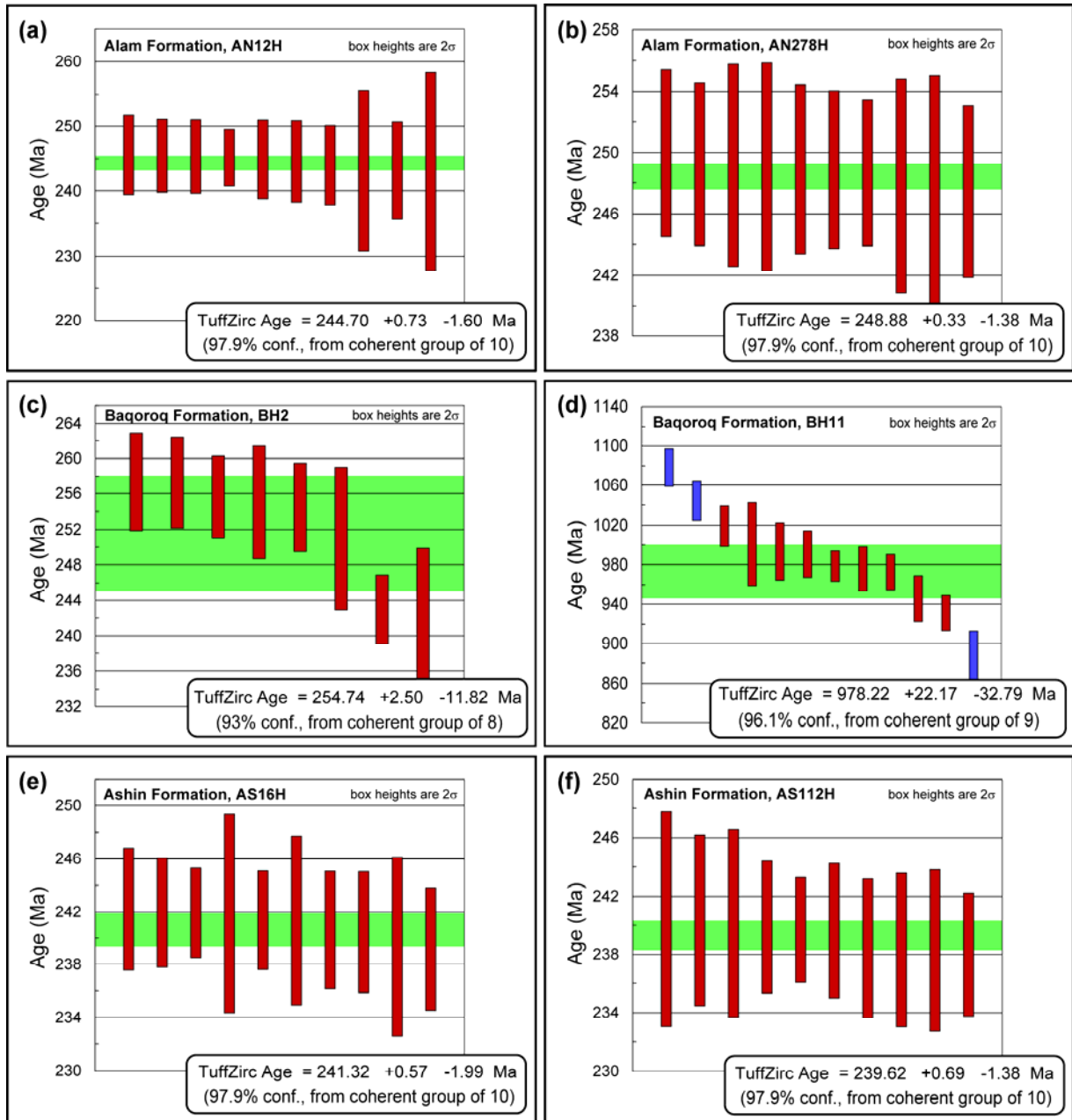


Figure 7

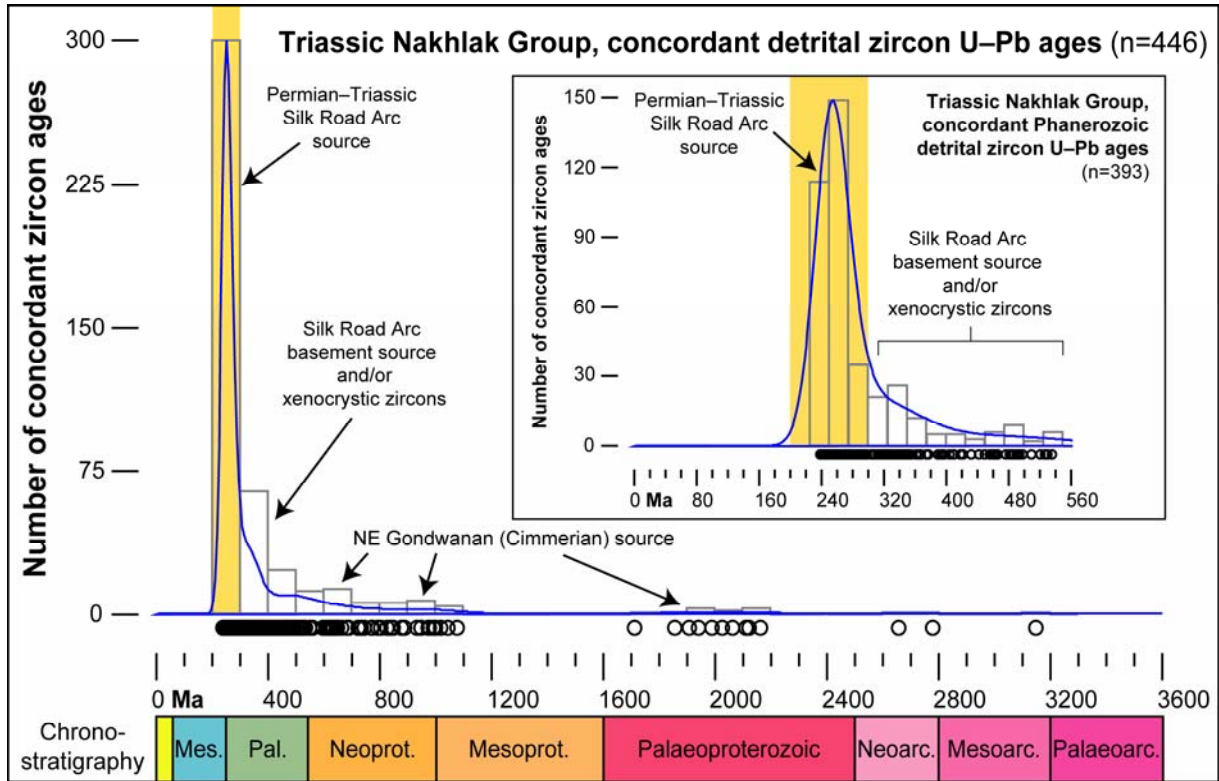


Figure 8

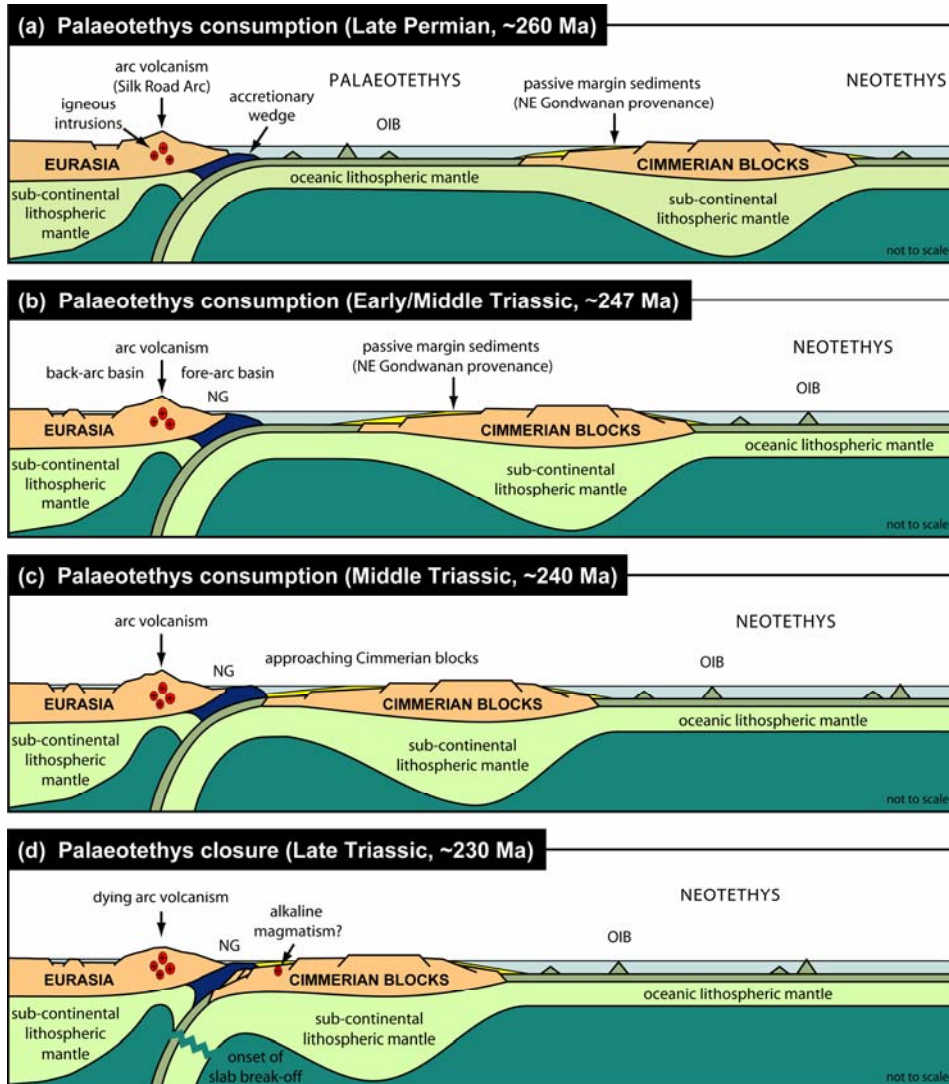


Figure 9

**Table 1**

Sample	Latitude	Longitude	Age	Stratigraphy	Rock type	No. of determined ages	No. of concordant ages	No. of concordant ages in %	Youngest concordant age (Ma)
AS112H	33° 34' 17.30"	53° 48' 47.12"	Upper Ladinian–?Lower Carnian	Ashin Formation	Lithic arkose	82	72	88	238 ± 4
AS16H	33° 34' 16.79"	53° 48' 23.95"	Upper Ladinian–?Lower Carnian	Ashin Formation	Arkose	85	84	99	239 ± 5
BH11	33° 33' 44.88"	53° 48' 26.07"	?Upper Anisian–Middle Ladinian	Baqoroq Formation	Lithic arkose	62	57	92	256 ± 7
BH2	33° 33' 45.67"	53° 47' 50.97"	?Upper Anisian–Middle Ladinian	Baqoroq Formation	Feldspathic litharenite	86	84	98	242 ± 7
AN278H	33° 33' 41.75"	53° 47' 49.33"	Middle Anisian	Alam Formation	Feldspathic litharenite	87	77	89	248 ± 6
AN12H	33° 32' 45.66"	53° 48' 45.42"	Olenekian–Anisian	Alam Formation	Litharenite	76	72	95	243 ± 15
Total:						478	446		
						100%	93%		